Hemodynamic Parameters in the Parent Arteries of Unruptured Intracranial Aneurysms Depend on Aneurysm Size and Are Different Compared to Contralateral Arteries: A 7 Tesla 4D Flow MRI Study

Rick J. van Tuijl, MSc,[1,2]* Kimberley M. Timmins, PhD,[1] Birgitta K. Velthuis, MD, PhD,[1]
Pim van Ooij, PhD,[3] Jaco J.M. Zwanenburg, PhD,[1,2] Ynte M. Ruigrok, MD, PhD,[4] and
Irene C. van der Schaaf, MD, PhD[1]

Background: Different Circle of Willis (CoW) variants have variable prevalences of aneurysm development, but the hemodynamic variation along the CoW and its relation to presence and size of unruptured intracranial aneurysms (UIAs) are not well known.

Purpose: Gain insight into hemodynamic imaging markers of the CoW for UIA development by comparing these outcomes to the corresponding contralateral artery without an UIA using 4D flow magnetic resonance imaging (MRI).

Study Type: Retrospective, cross-sectional study.

Subjects: Thirty-eight patients with an UIA, whereby 27 were women and a mean age of 62 years old.

Field Strength/Sequence: Four-dimensional phase-contrast (PC) MRI with a 3D time-resolved velocity encoded gradient echo sequence at 7 T.

Assessment: Hemodynamic parameters (blood flow, velocity pulsatility index [vPI], mean velocity, distensibility, and wall shear stress [peak systolic (WSS_{MAX}), and time-averaged (WSS_{MEAN})]) in the parent artery of the UIA were compared to the corresponding contralateral artery without an UIA and were related to UIA size.

Statistical Tests: Paired *t*-tests and Pearson Correlation tests. The threshold for statistical significance was $P < 0.05$ (two-tailed).

Results: Blood flow, mean velocity, WSS_{MAX}, and WSS_{MEAN} were significantly higher, while vPI was lower, in the parent artery relative to contralateral artery. The WSS_{MAX} of the parent artery significantly increased linearly while the WSS_{MEAN} decreased linearly with increasing UIA size.

Conclusions: Hemodynamic parameters and WSS differ between parent vessels of UIAs and corresponding contralateral vessels. WSS correlates with UIA size, supporting a potential hemodynamic role in aneurysm pathology.

Level of Evidence: 2

Technical Efficacy: Stage 2

About 3% of the population has an unruptured intracranial aneurysm (UIA) and, due to the increasing availability and quality of brain imaging, the number of incidentally discovered UIAs is increasing.[1] Rupture of an UIA results in an aneurysmal subarachnoid hemorrhage (ASAH), which is a devastating type of stroke with a 35% case fatality and 35% render dependent.[2] Insight into hemodynamic imaging markers of the Circle of Willis (CoW) for UIA development and growth may aid in clinical decision-making to determine UIAs with a high rupture risk, which might then undergo preventive treatment.

The pathogenesis of UIA development remains insufficiently understood.[3] Altered hemodynamics is one of the most widely accepted hypotheses contributing to aneurysmal development and growth, in which hemodynamic wall shear stress (WSS) contributes to pathophysiologic remodeling of the vessel wall.[4–6] Several studies related intra-aneurysmal hemodynamics to aneurysmal size and growth, in which the most established hemodynamic parameters associated with UIA were complex flows, concentrated areas of high WSS, or frictional forces.[6–8] It is known that variations in the configuration of the CoW, with concomitant hemodynamic variations, are related to aneurysmal development.[9] Novel imaging techniques such as four-dimensional (4D) flow at 7 Tesla (7 T) magnetic resonance imaging (MRI) enable accurate and reproducible measurement and quantification of blood flow and the resulting WSS, mean velocity, velocity pulsatility index (vPI), and the arterial distensibility of the intracranial vessels.[10,11]

This study aimed to compare the hemodynamics parameters in the parent artery of the UIA to the corresponding contralateral artery without an UIA, using 7 T 4D flow MRI. In addition, this study aimed to assess the potential relation between hemodynamic parameters and UIA size, in order to obtain insight in a possible hemodynamic role in aneurysmal development.

Methods

Patients

The local ethics review committee approved the study and written informed consent was obtained from all participants. This study included participants with an UIA from the ERASE (**E**arly **R**ecognition of persons at high risk of **A**neurysmal **S**ubarachnoid hemorrhag**E**) study, a screening study for UIA in family members of patients with an UIA in the University Medical Center Utrecht. In case an UIA was identified in this study an additional 7 T MRI was performed. Patients with UIAs larger than 4 mm of size were included from the Flow@Aneurysm study. For inclusion in this study the UIA locations needed to have a parent artery with a comparable contralateral artery without an UIA and a successful 7 T 4D flow scan of the CoW. A total of 50 patients were

scanned using 7 T MRI. Twelve patients were excluded due to inability to perform ipsilateral versus contralateral comparison for the following reasons: 1) aneurysms on both sides (4×); 2) basilar artery aneurysm (2×); 3) anterior communicating (Acom) aneurysms located in the middle (3×); 4) UIA that was later diagnosed as an infundibulum (2×); and 5) a posterior inferior cerebral artery (PICA) aneurysm that was outside the field of view of the 4D flow scan (1×).

In total, 38 patients with an UIA who had undergone a 4D flow imaging were included on a 7 T MRI scanner (Philips). Two-dimensional (2D) measurements (i.e., size measurements in a single plane in which the aneurysm appeared largest) of all the UIAs were performed manually on the IntelliSpace (Philips Healthcare, Best, The Netherlands) by a neuroradiologist (IvdS with over 15 years of experience). These measurements were performed based on previous studies showing good to excellent inter and intraobserver 2D size measurements for the height and width of the UIA.[12] The UIA length and width were measured on the 3 T TOF-MRAs on a 0.1-mm scale using electronic calipers (provided by DICOM viewing software). In case of anterior communicating artery (Acom) aneurysms, the aneurysm had to be clearly located at either the left or the right side of the Acom/anterior cerebral artery (ACA) bifurcation, such that one ACA was identifiable as the parent artery and the other could serve as control. This population only included patients with common CoW variants that are present in >5% of the normal population (i.e., a complete CoW or a CoW with a missing or hypoplastic (<1 mm) Acom or posterior communicating artery (Pcom) determined by evaluating the TOF-MRA by RvT).[13] Patients with previous treatment of additional aneurysms were also excluded as this treatment may influence CoW hemodynamics.

MRI Acquisition

Participants underwent 7 T MRI (Philips Healthcare, Best, The Netherlands) using a volume transmit and 32-Channel receive coil (Nova Medical, Houston, United States). For this study, the Amsterdam Medical Center "PROspective Undersampling in multiple Dimensions" (PROUD) software patch was used, which enables a pseudospiral k_y/k_z-plane acquisition scheme designed for incoherent undersampling with a variable sampling density.[14]

Time-resolved 3D phase-contrast (PC) velocity maps (4D flow scan) over the cardiac cycle were acquired with the following parameters: angulated coronal field of view 250 (feet–head) × 190 (right–left) × 20 (anterior–posterior)-mm^3, acquired resolution of $0.7 \times 0.7 \times 0.7$ mm^3, repetition time/echo time = 6.4/2.2, velocity encoding sensitivity 100 cm/s, flip angle 15°, nominal acceleration factor 7, and 12 reconstructed cardiac phases (i.e., reconstructed temporal resolution 83 msec for a heart rate of 60 bpm). Retrospective gating used a peripheral pulse unit for heartbeat detection.

Acquisition duration was 10 minutes. Vendor-supplied image-based shimming was performed using second-order terms, before acquiring the 4D flow scan.
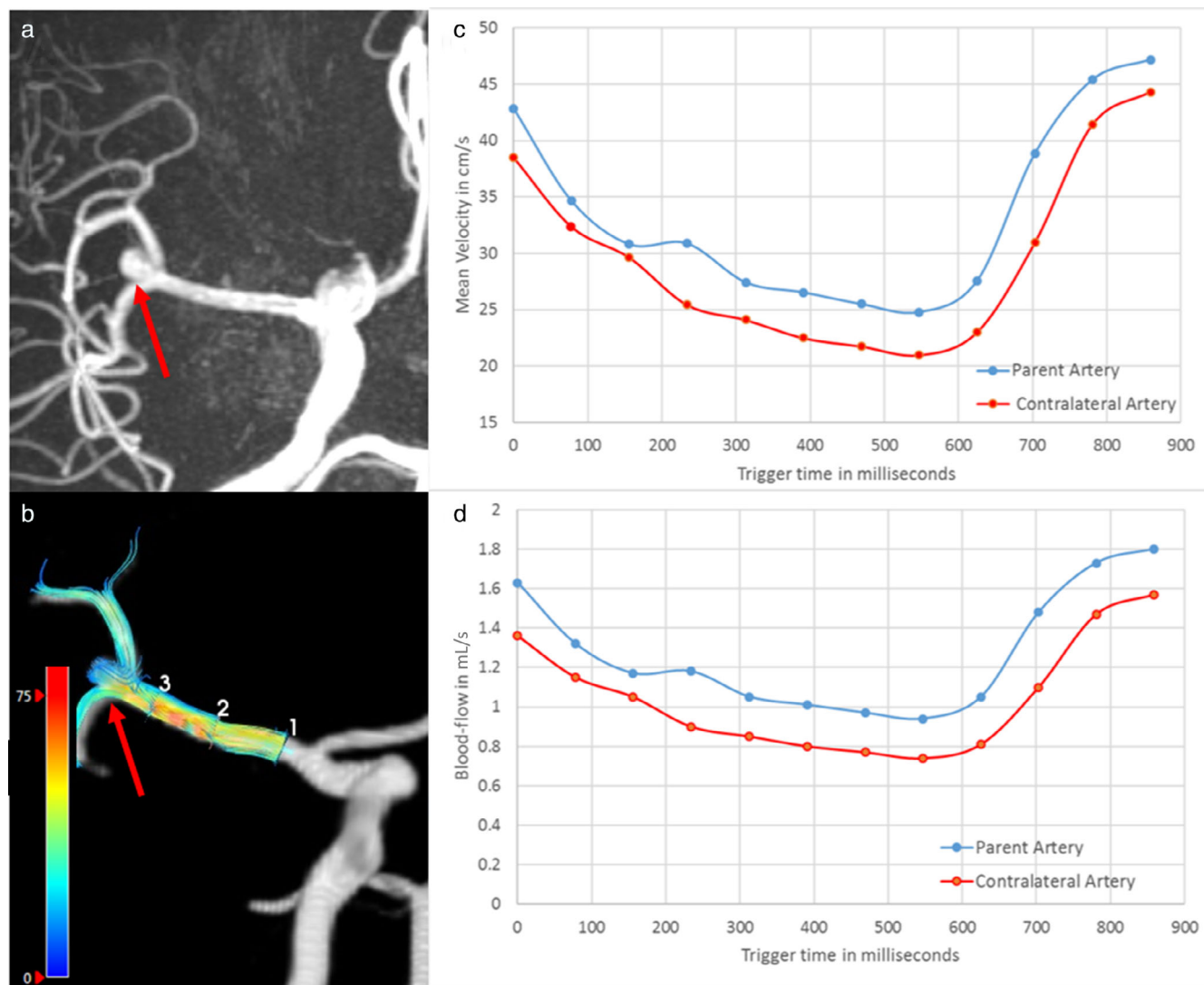
4D Flow Analysis

4D flow datasets were analyzed by RvT (with 4 years of 4D flow analysis experience) using CAAS MR Solutions v5.1.2 software (Pie Medical Imaging, Maastricht, The Netherlands). Automatic background phase correction and anti-aliasing correction was performed in the CAAS software for all 4D flow datasets. Given that no velocity aliasing was observed, the default antialiasing step in CAAS did not affect the 4D flow data. CAAS automatically generates the centerline along the complete CoW from the ICA toward the smaller cerebral arteries and perpendicular slices are manually set. Three slices along the ipsilateral and contralateral artery were placed around 10%, 50%, and 90% (Fig. 1b, slice 1 [10%] slice 2 [50%], and slice 3 [90%]) of the length of the vessel. These perpendicular slices were visually checked and automatically propagated to create volumetric blood flow rate traces (mL/s) and separate velocity (cm/s) traces over the cardiac cycle. The blood-flow velocity pulsatility index was calculated from each velocity trace as defined in Eq. 1.

$$\left(vPI = \left(Velocity_{max} - Velocity_{min} \right) / Velocity_{mean} \right) \quad (1)$$

The arterial distensibility in kilopascal $(kPa)^{-1}$ was calculated from each area curve, where A indicates the area of the arterial lumen region of interest (ROI) at end-diastole, ΔA is the stroke change in lumen area over the cardiac cycle.

FIGURE 1: Representation of the 4D flow image analysis regarding the parent vessel with the aneurysm versus the contralateral side without aneurysm using CAAS software. (a) MRA TOF image to show the middle cerebral artery aneurysm (red arrow) in this subject. (b) Blood-flow analysis using in the same patient focused on the parent artery. The streamlines illustrate the blood flow, with colors depending on the local velocity. (c) Mean velocity curves (in cm/s) for this subject in the parent (blue) and contralateral artery (red). (d) Blood-flow (in mL/s) for this subject in the parent (blue) and contralateral artery (red).

TABLE 1. Baseline Characteristics of the 38 Included Subjects

Characteristics	
No. of patients	38
No. of aneurysms	38
Women	27 (71%)
Age, years $\pm$ SD	62 $\pm$ 12
Aneurysm size (mean) (mm $\pm$ SD)	5.2 $\pm$ 2.4
UIA location	
Middle cerebral artery	20 (52.6%)
Internal carotid artery	9 (23.7%)
Anterior communicating artery	9 (23.7%)

UIA = unruptured intracranial aneurysm; SD = standard deviation.

ΔP is systolic pressure − diastolic pressure, which was obtained from patient dossiers as described in Eq. 2.

$$(= \Delta A/(A \times \Delta P)) \tag{2}$$

The diameter at end diastole was calculated from A, assuming a circular ROI. The inter-examination, inter-observer, and intra-observer reliability of the analysis with the CAAS software in the CoW have been tested previously with good to very good reproducibility and repeatability (ICC = 0.65–0.96).[15–17]

Wall Shear Stress Measurements

WSS was calculated using an in-house-developed software in Matlab R2018a (The Mathworks, Inc.) by multiplying the wall shear rate by the dynamic viscosity of blood (3.2×10^{-3} Pa·s).[18] WSS traces over the cardiac cycle were calculated for a user-defined region of interest (ROI), whereby the ROI was aligned along the whole parent artery, without including the UIA. Each time point in the WSS trace represented the spatial mean WSS of the ROI. The same was done for the contralateral side by placing the ROI along the ipsilateral artery. Two WSS parameters were obtained from the WSS traces: the WSS at peak systole (WSS_{MAX}) and the time-averaged WSS (WSS_{MEAN}), in which the WSS is expressed as the average over the cardiac cycle. The outcome parameters blood flow, vPI, mean velocity, WSS_{MAX}, WSS_{MEAN}, arterial distensibility, and mean lumen area over the cardiac cycle were calculated (Fig. 1) for both the parent artery of the UIA and the corresponding contralateral artery.

Statistical Analysis

Normality of data was tested using the Kolmogorov–Smirnov test. The obtained values for pulsatility index, distensibility, mean velocity, lumen area, and diameter were averaged over the three slices. The three slices are averaged together since these slices did not differ significantly from each other. This has been studied and described in a previous study focusing on the relation between A1-diameter asymmetry and blood flow.[17] The hemodynamics (blood flow, vPI, mean velocity, arterial distensibility, mean lumen area, WSS_{MAX}, and WSS_{MEAN}) in the parent vessel of the UIA (ipsilateral) were compared to the contralateral artery without an UIA, using a paired t-test. These analyses were done for all UIA locations grouped together and per UIA location. Next, the relationship between the WSS (WSS_{MAX} and WSS_{MEAN}) in the parent artery of the UIA and UIA size were studied, by creating a scatterplot, and assessing correlation using the Pearson correlation test. Additionally, hemodynamic differences per UIA location have been studied using a multivariate analysis with UIA location as fixed factor to study UIA size influence. The statistical significance threshold was set at $P < 0.05$. All statistical analyses were performed in IBM Statistics Package of Social Sciences (SPSS) (Version 25, IBM, Armonk, NY, USA).

Results

Baseline Characteristics

In the 38 patients (27 women, mean age 62 ± 12 years; Table 1), the UIA location was as follows: 20 at the middle cerebral artery (MCA), 9 at the internal carotid artery (ICA), and 9 at the anterior communicating artery (Acom). Six of the nine ICA UIAs were located at the origin of the ophthalmic artery, two at the posterior communicating artery, and one at the ICA top. All nine Acom UIAs were located either at the left or right side where the Acom connects to the A1–A2 segments of the anterior cerebral artery. Size of the UIA ranged from 1.5 mm to 11 mm (mean size $\pm$ SD per location (mm); MCA = 5.5 ± 2.6; ICA = 5.3 ± 2.8, and Acom = 4.5 ± 1.5) (Table 1). The mean values (with standard deviations) of the blood flow, mean velocity, vPI, arterial distensibility, WSS_{MAX}, WSS_{MEAN}, and mean lumen area for all UIA locations together, and for the three different UIA locations separately, are given in Table 2. All hemodynamic parameters measurements were normally distributed (Supplementary Table S1).

Hemodynamic Parameters for Parent Vessel of UIA Versus Contralateral Artery

The blood flow, mean velocity, WSS_{MAX}, and WSS_{MEAN} were significantly higher in the parent artery containing an UIA compared to the contralateral artery, for all UIA locations together and separately (MCA, ICA, and Acom). Conversely, the vPI was statistically significantly lower at the ipsilateral side compared to the contralateral side for all

TABLE 2. Hemodynamic Parameters (±Standard Deviation) of the Parent Artery of the Unruptured Intracranial Aneurysm (UIA) and the Contralateral Side for All UIA Together and Per Aneurysm Location

All UIA ($N = 38$)			
	Parent artery	**Contralateral**	**P-value**
WSS_{MAX} (Pa)	9.90 ± 1.33	7.42 ± 1.11	<0.001
WSS_{MEAN} (Pa)	2.65 ± 0.77	2.13 ± 0.83	<0.001
Blood flow (mL/s)	1.35 ± 0.69	1.09 ± 0.68	<0.001
vPI	0.83 ± 0.15	0.97 ± 0.15	<0.001
Mean velocity (cm/s)	33.06 ± 8.17	28.46 ± 7.11	<0.001
Distensibility ($kPa^{-1} \times 10^{-3}$)[a]	29.66 ± 6.19	28.58 ± 5.08	0.40
Mean lumen area (mm^2)	5.69 ± 3.36	5.21 ± 3.60	0.02
MCA ($N = 20$)			
WSS_{MAX} (Pa)	9.92 ± 1.33	7.13 ± 1.22	<0.001
WSS_{MEAN} (Pa)	2.65 ± 0.85	2.20 ± 1.00	0.002
Blood flow (mL/s)	1.13 ± 0.23	0.86 ± 0.20	<0.001
vPI	0.85 ± 0.13	0.96 ± 0.15	0.001
Mean velocity (cm/s)	32.65 ± 8.86	29.19 ± 7.25	0.015
Distensibility ($kPa^{-1} \times 10^{-3}$)	26.51 ± 4.10	25.93 ± 3.52	0.28
Mean lumen area (mm^2)	4.25 ± 0.86	4.21 ± 0.91	0.45
ICA ($N = 9$)			
WSS_{MAX} (Pa)	10.01 ± 1.53	7.76 ± 0.76	0.001
WSS_{MEAN} (Pa)	2.53 ± 0.57	2.00 ± 0.65	<0.001
Blood flow (mL/s)	2.46 ± 0.25	2.16 ± 0.29	0.009
vPI	0.79 ± 0.07	0.97 ± 0.09	<0.001
Mean velocity (cm/s)	32.22 ± 7.10	29.52 ± 6.23	0.182
Distensibility ($kPa^{-1} \times 10^{-3}$)	34.43 ± 6.58	33.13 ± 4.28	0.76
Mean lumen area (mm^2)	10.40 ± 2.10	10.50 ± 2.11	0.89
Acom ($N = 9$)			
WSS_{MAX} (Pa)	9.74 ± 1.02	7.69 ± 1.03	<0.001
WSS_{MEAN} (Pa)	2.65 ± 0.75	2.12 ± 0.51	<0.001
Blood flow (mL/s)	0.74 ± 0.16	0.49 ± 0.27	0.006
vPI	0.83 ± 0.24	0.98 ± 0.21	0.015
Mean velocity (cm/s)	34.31 ± 7.92	25.32 ± 6.88	0.007
Distensibility ($kPa^{-1} \times 10^{-3}$)	29.99 ± 5.22	28.18 ± 4.67	0.78
Mean lumen area (mm^2)	2.69 ± 0.44	1.65 ± 0.60	0.001

UIA = unruptured intracranial aneurysm; WSS_{MAX} = peak systolic wall shear stress; WSS_{MEAN} = time-averaged wall shear stress; vPI = velocity pulsatility index; Acom = anterior communicating artery; ICA = internal carotid artery; MCA = middle cerebral artery.
[a]The distensibility was computed using systemic pressure measurements with a pressure cuff, as invasive intraluminal pressures were not available.
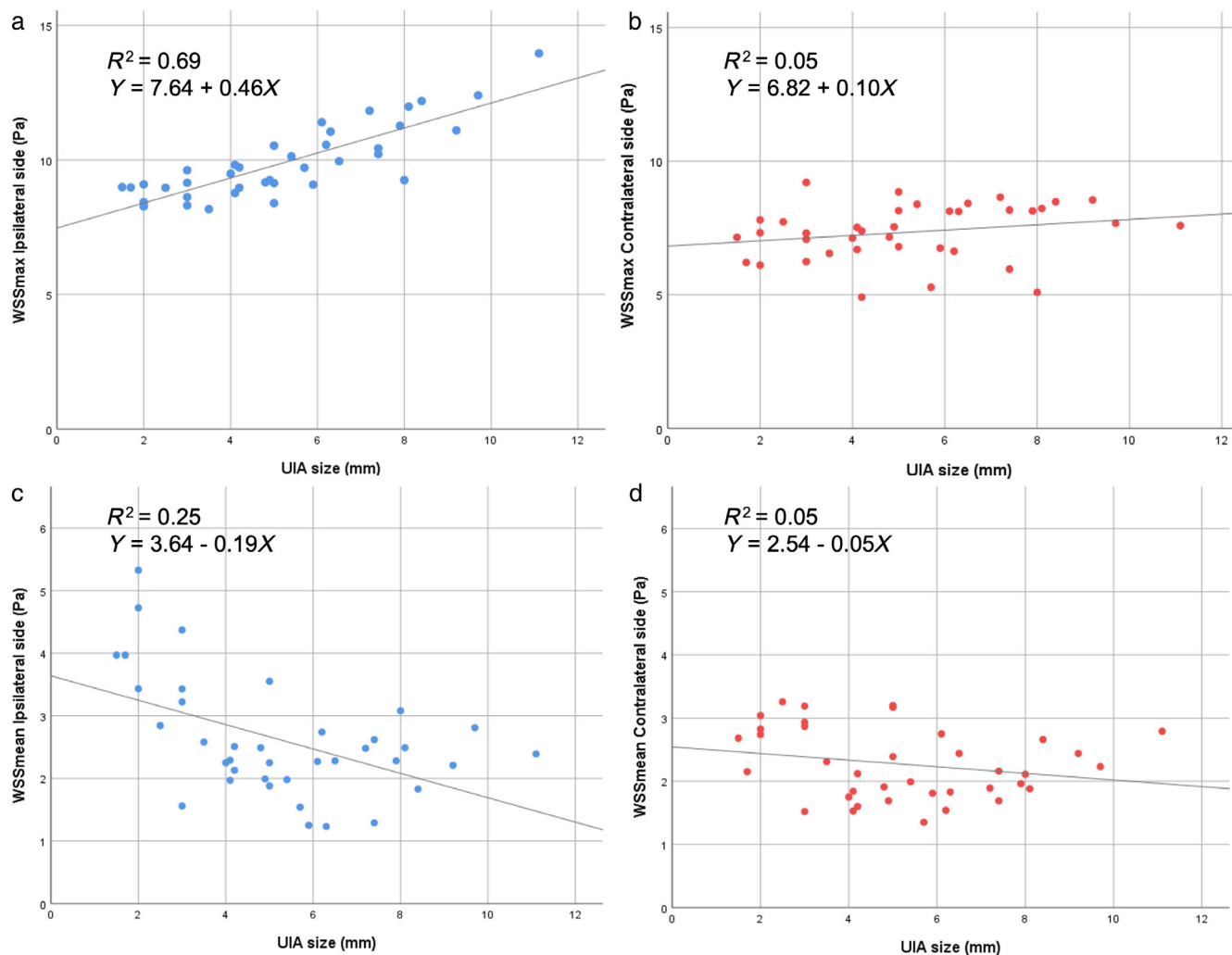
FIGURE 2: Peak-systolic wall shear stress (WSS_{MAX}) (**a** and **b**) in blue and time-averaged wall shear stress (WSS_{MEAN}) (**c** and **d**) in red (Pascal) related to aneurysm size (mm) for all 38 included unruptured intracranial aneurysms (UIA). (a) WSS_{MAX} in the parent vessel containing an UIA is shown with a trend line ($Y = 7.46 + 0.46X$) ($R^2 = 0.69$, $P < 0.001$). (b) The WSS_{MAX} in the contralateral vessel without an UIA ($Y = 6.82 + 0.10X$) ($R^2 = 0.05$, $P = 0.16$). (c) The WSS_{MEAN} in the parent vessel containing an UIA is shown with a trend line ($Y = 3.64–0.19X$) ($R^2 = 0.25$, $P < 0.001$). (d) The WSS_{MEAN} in the contralateral vessel without an UIA is shown and a trend line ($Y = 2.54–0.05X$) ($R^2 = 0.05$, $P = 0.17$).

different UIA locations (Table 2). The mean lumen area was statistically significantly higher in the parent artery containing an Acom UIA compared to the contralateral artery, but no difference was seen for the other UIA locations. There were no statistically significant differences in arterial distensibility for any UIA location.

Relationship Between WSS and UIA Size

The WSS_{MAX} of the parent artery of the UIA increased linearly with increasing UIA size (Fig. 2), with statistically significant correlation ($R^2 = 0.69$, Pearson correlation coefficient of 0.84). The WSS_{MEAN} of the parent artery of the UIA decreased linearly with increasing UIA size, with statistically significant correlation ($R^2 = 0.25$, Pearson correlation coefficient of −0.56).

No significant hemodynamic differences were found for the different UIA locations related to UIA size ($P > 0.12$).

The contralateral artery showed no statistically significant correlation with UIA size.

Discussion

In the parent artery containing an UIA the blood flow, mean velocity, WSS_{MAX}, and WSS_{MEAN} were higher and, conversely, vPI was lower compared to the contralateral artery. The WSS_{MAX} of the parent artery increased linearly with increasing UIA size, whereas the average WSS over the whole parent artery decreased with increasing UIA size. There were no significant differences in arterial distensibility for any UIA location.

A systematic review investigating hemodynamics and the relation between computational fluid dynamics (CFD) in the CoW and UIA formation, growth, or rupture with three case series on 13 aneurysms in total.[19] Due to limited

number of cases and the heterogeneity between the three different case series, no conclusion was drawn in this review on the relation between hemodynamics and development and instability of UIAs. Another study, applying 3 T 2D phase-contrast MRI in 96 patients to study aneurysmal parent artery-specific inflow waveforms for different CoW configurations found that inflow conditions vary substantially between aneurysmal parent arteries and different forms of CoW configurations.[20] The regional hemodynamic forces probably predispose to vessel wall remodeling and eventually to the development and growth of UIAs.[21] This is in line with the findings from this study that hemodynamics in the parent vessel of the UIA is different from the contralateral side.

Some specific locations or variations in the CoW have been reported to be associated with aneurysmal development, growth, and rupture through hemodynamic effects.[19] Vessel bifurcations, and specifically the branch forming a smaller angle with the parent artery, are associated with aneurysmal presence.[22] This study confirms asymmetry in the A1-segment by showing an increased lumen area of the ipsilateral anterior cerebral arteries, which is associated with a higher prevalence of Acom UIA as compared to symmetric A1-segments.[23] No significant difference in area was seen for MCA and ICA UIA, suggesting no such asymmetry as in the A1 segments.

The relation between aneurysm size and hemodynamic parameters in the parent artery has been described before in one case report of a patient with eight small (<7 mm) UIAs using CFD.[24] Its findings are in accordance with these results, showing a linear correlation between aneurysm size and the flow rate in the parent artery. A previous study reported a negative linear relation between average WSS_{MEAN}, measured in the UIA itself at peak systole, and UIA size that was independent of UIA location.[25] Another study that studied hemodynamic differences between ruptured and unruptured aneurysms showed statistically significantly lower minimum WSS and WSS_{MEAN} in the parent artery of ruptured aneurysms.[26] This is the first MRI flow study that compared the hemodynamic parameters in both the ipsilateral parent arteries and contralateral sides of the CoW and to relate this to UIA size. This study showed that both WSS_{MAX} and WSS_{MEAN} were higher in the ipsilateral parent artery compared to the contralateral side and showed that a positive linear correlation was seen between WSS_{MAX} and UIA size, whereas WSS_{MEAN} in the parent artery was negatively correlated to UIA size. The relation between WSS and UIA implies that there is a relatively low WSS_{MAX} and high WSS_{MEAN} in parent arteries of small UIA, whereas a relatively high WSS_{MAX} and low WSS_{MEAN} are found in large UIAs. No such trend was seen at the contralateral side without an UIA, which was used as a reference measurement. As WSS_{MEAN} both in the parent artery and in the UIA itself is negatively correlated with aneurysm size and WSS_{MEAN} is

lower in parent arteries of ruptured aneurysms, WSS_{MEAN} might be a better marker than WSS_{MAX} to use in imaging of UIAs. In contrast, it has been reported that high WSS can initiate cascades of biochemical signals within the vessel wall through endothelium-mediated mechanotransduction and trigger aneurysm initiation.[6] The findings of this study are consistent with the notion of an effect of abnormal flow on endothelial cells, and the formation of UIA in regions with abnormal WSS. Also, the lack of differences in distensibility, as a measure of compliance, between the parent artery and the contralateral artery, seems to point to factors external to the vessel wall for the initiation of aneurysm formation.

The results of this study may have implications for the boundary setting for CFD in patients with UIA. In CFD, the simulations remain mathematical and input data is derived from literature, generally from healthy subjects.[24] The different hemodynamics in the parent artery containing an UIA compared to the contralateral side implies that literature-based input, as inflow boundary conditions from healthy subjects, might not give realistic CFD-derived hemodynamics in an UIA population.[27] Therefore, further studies to derive CFD boundaries from in vivo 4D flow imaging in a larger UIA patient population are necessary. Furthermore, in vivo derived data on hemodynamics in the CoW in patients with an UIA offers the opportunity for validation studies with computational flow models. Finally, future studies with longitudinal data (i.e., follow-up imaging) on hemodynamics in the CoW will give insight in the sequential interactions of hemodynamics in the CoW and aneurysmal formation, growth, and rupture. Moreover, it will also provide an answer to the question whether the hemodynamic differences between the parent artery containing an UIA and the contralateral artery observed are the cause or the consequence of the UIA. We expect that the hemodynamic differences between vessels reflect differences in the size of the flow territories of the vessels, which is known to vary between individuals.[28]

Limitations

This single center, single magnet, single vendor cross-sectional cohort study design does not allow conclusions to be made on whether the presence and size of UIAs cause the observed hemodynamic differences in the parent vessel, or if UIAs are rather the result of (pre-existent) hemodynamic differences in the parent vessel. Also, CoW variations in patients included in this study may have resulted in some hemodynamic differences in the vessels of the CoW. To partly account for this, only patients with common CoW variants[13] were included. Given the small diameters of the arteries relative to the resolution of the 4D flow scan, the reported values might suffer from partial volume effects. However as both the ipsi- and contralateral arteries were measured and analyzed in the same way, the observed differences between both sides reflect true hemodynamic differences. For the distensibility, ideally the

pressure inside the lumen at the location of interest is preferred but these measurements are invasive and scarce. Therefore, in this study, the distensibility measurements take the systolic and diastolic pressure into account.

Conclusion

Hemodynamic parameters and WSS may differ between parent vessels of UIA and the corresponding contralateral vessels while maximum WSS correlates to aneurysm size. These findings support the hypothesis that hemodynamic forces predispose to vessel wall remodeling and eventually to the development of UIAs. However, whether the differences in hemodynamics are the cause or the consequence of UIA needs to be studied further.

References

1. Gabriel RA, Kim H, Sidney S, et al. Ten-year detection rate of brain arteriovenous malformations in a large, multiethnic, defined population. Stroke 2010;41:21-26. https://doi.org/10.1161/STROKEAHA.109.566018.

2. Nieuwkamp DJ, Setz LE, Algra A, Linn FH, de Rooij NK, Rinkel GJ. Changes in case fatality of aneurysmal subarachnoid haemorrhage over time, according to age, sex, and region: A meta-analysis. Lancet Neurol 2009;8:635-642. https://doi.org/10.1016/S1474-4422(09)70126-7.

3. Kancheva AK, Velthuis BK, Ruigrok YM. Imaging markers of intracranial aneurysm development: A systematic review. J Neuroradiol 2021;49:1-6. https://doi.org/10.1016/j.neurad.2021.09.001.

4. Szajer J, Ho-Shon K. A comparison of 4D flow MRI-derived wall shear stress with computational fluid dynamics methods for intracranial aneurysms and carotid bifurcations—A review. Magn Reson Imaging 2018;48:62-69. https://doi.org/10.1016/j.mri.2017.12.005.

5. Lu D, Kassab GS. Role of shear stress and stretch in vascular mechanobiology. J R Soc Interface 2011;8:1379-1385. https://doi.org/10.1098/rsif.2011.0177.

6. Meng H, Tutino VM, Xiang J, Siddiqui A. High WSS or low WSS? Complex interactions of hemodynamics with intracranial aneurysm initiation, growth, and rupture: Toward a unifying hypothesis. Am J Neuroradiol 2014;35:1254-1262. https://doi.org/10.3174/ajnr.A3558.

7. Leemans EL, Cornelissen BMW, Slump CH, Majoie CBLM, Cebral JR, Marquering HA. Comparing morphology and hemodynamics of stable-versus-growing and grown intracranial aneurysms. Am J Neuroradiol 2019;40:2102-2110. https://doi.org/10.3174/ajnr.A6307.

8. Chung BJ, Mut F, Putman CM, et al. Identification of hostile hemodynamics and geometries of cerebral aneurysms: A case-control study. Am J Neuroradiol 2018;39:1860-1866. https://doi.org/10.3174/ajnr.A5764.

9. Tang H, Wang Q, Xu F, et al. Underlying mechanism of hemodynamics and intracranial aneurysm. Chin Neurosurg J 2021;7:1-8. https://doi.org/10.1186/s41016-021-00260-2.

10. Van Ooij P, Zwanenburg JJM, Visser F, et al. Quantification and visualization of flow in the Circle of Willis: Time-resolved three-dimensional phase contrast MRI at 7 T compared with 3 T. Magn Reson Med 2013;69:868-876. https://doi.org/10.1002/mrm.24317.

11. van Tuijl RJ, Ruigrok YM, Geurts LJ, et al. Does the internal carotid artery attenuate blood-flow pulsatility in small vessel disease? A 7 T 4D-flow MRI study. J Magn Reson Imaging 2022;56:527-535. https://doi.org/10.1002/jmri.28062.

12. Timmins KM, Kuijf HJ, Vergouwen MDI, et al. Reliability and agreement of 2D and 3D measurements on MRAs for growth assessment of unruptured intracranial aneurysms. Am J Neuroradiol 2021;42:1598-1603. https://doi.org/10.3174/ajnr.A7186.

13. Hindenes LB, Håberg AK, Johnsen LH, Mathiesen EB, Robben D, Vangberg TR. Variations in the circle of willis in a large population sample using 3D TOF angiography: The Tromsø study. PLoS One 2020;15:1-15. https://doi.org/10.1371/journal.pone.0241373.

14. Gottwald LM, Töger J, Markenroth Bloch K, et al. High spatiotemporal resolution 4D flow MRI of intracranial aneurysms at 7T in 10 minutes. Am J Neuroradiol 2020;41:1201-1208. https://doi.org/10.3174/AJNR.A6603.

15. Juffermans JF, Westenberg JJM, van den Boogaard PJ, et al. Reproducibility of aorta segmentation on 4D flow MRI in healthy volunteers. J Magn Reson Imaging 2021;53:1268-1279. https://doi.org/10.1002/jmri.27431.

16. Van Ooij P, Powell AL, Potters WV, Carr JC, Markl M, Barker AAJ. Reproducibility and interobserver variability of systolic blood flow velocity and 3D wall shear stress derived from 4D flow MRI in the healthy aorta. J Magn Reson Imaging 2016;43:236-248. https://doi.org/10.1002/jmri.24959.

17. van Tuijl RJ, Ruigrok YM, Ophelders MEH, et al. Relationship between diameter asymmetry and blood flow in the pre-communicating (A1) segment of the anterior cerebral arteries. J Neuroradiol 2022;15:S010-9861(22)00156-0. https://doi.org/10.1016/j.neurad.2022.10.004.

18. Václavů L, Baldew ZAV, Gevers S, et al. Intracranial 4D flow magnetic resonance imaging reveals altered haemodynamics in sickle cell disease. Br J Haematol 2018;180:432-442. https://doi.org/10.1111/bjh.15043.

19. Shen Y, Molenberg R, Bokkers RPH, Wei Y, Uyttenboogaart M, van Dijk JMC. The role of hemodynamics through the Circle of Willis in the development of intracranial aneurysm: A systematic review of numerical models. J Pers Med 2022;12:1008. https://doi.org/10.3390/jpm12061008.

20. Cornelissen BMW, Schneiders JJ, Sprengers ME, et al. Aneurysmal parent artery-specific inflow conditions for complete and incomplete circle of willis configurations. Am J Neuroradiol 2018;39:910-915. https://doi.org/10.3174/ajnr.A5602.

21. Rayz VL, Cohen-Gadol AA. Hemodynamics of cerebral aneurysms: Connecting medical imaging and biomechanical analysis. Annu Rev Biomed Eng 2020;22:231-256. https://doi.org/10.1146/annurev-bioeng-092419-061429.

22. Gao BL, Hao H, Hao W, Ren CF, Yang L, Han Y. Cerebral aneurysms at major arterial bifurcations are associated with the arterial branch forming a smaller angle with the parent artery. Sci Rep 2022;12:1-10. https://doi.org/10.1038/s41598-022-09000-7.

23. Krasny A, Nensa F, Sandalcioglu IE, et al. Association of aneurysms and variation of the A1 segment. J Neurointerv Surg 2014;6:178-183. https://doi.org/10.1136/neurintsurg-2013-010669.

24. Jou L, Britz G. Correlation between aneurysm size and hemodynamics in one individual with multiple small intracranial aneurysms. Cureus 2016;8:e683. https://doi.org/10.7759/cureus.683.

25. Zhang M, Peng F, Li Y, He L, Liu A, Li R. Associations between morphology and hemodynamics of intracranial aneurysms based on 4D flow and black-blood magnetic resonance imaging. Quant Imaging Med Surg 2021;11:597-607. https://doi.org/10.21037/QIMS-20-440.

26. Detmer FJ, Chung BJ, Jimenez C, Hamzei-sichani F, Putman C, Cebral JR. Associations of hemodynamics, morphology, and patient characteristics with aneurysm rupture stratified by aneurysm location. Neuroradiology 2019;61:275-284. https://doi.org/10.1007/s00234-018-2135-9.Associations.

27. Rajabzadeh-Oghaz H, van Ooij P, Veeturi SS, Tutino VM, Zwanenburg JJ, Meng H. Inter-patient variations in flow boundary conditions at middle cerebral artery from 7T PC-MRI and influence on computational fluid dynamics of intracranial aneurysms. Comput Biol Med 2020;120:103759. https://doi.org/10.1016/j.compbiomed.2020.103759.

28. van Laar PJ, Hendrikse J, Golay X, Lu H, van Osch MJ, van der Grond J. In vivo flow territory mapping of major brain feeding arteries. Neuroimage 2006;29(1):136-144. https://doi.org/10.1016/j.neuroimage.2005.07.011.